Contaminant concentration on pipe walls following radial jet injection: a computational fluid dynamics approach

R. S. Neve
Thermo-Fluids Engineering Research Centre, Department of Mechanical Engineering and Aeronautics, City University, London, UK

A computational fluid dynamics technique has been used to predict the likely concentration levels along a pipe wall of chemicals injected radially from a nozzle. No published empirical data appear to be available, despite the importance of this subject in protecting pipe walls in the vicinity of the dosing point if the chemicals and pipe materials are incompatible. Validation of predictions is by comparison with experimental data for other parameters related to the flow. Where possible, results have been analyzed and presented in dimensionless form so that the article can act as a more generally useful design guide.

Keywords: pipes; injection; contaminants; diffusion; protection

Introduction

The method of injecting a tracer fluid from a point source at a pipe wall has been used for many years for bulk flow measurement in the pipe. For a known tracer volumetric flow rate and concentration, a measure of the resulting concentration at a very large distance downstream, where the tracer is assumed to have fully diffused, enables the conveyed fluid flow rate to be calculated. However, if the nominal point source is replaced by a more substantial jet, the same technique allows the contaminant fluid in the jet to be mixed with the bulk fluid; for example, in the chlorination of water. In this latter case, the volumetric flow rate in the jet must clearly be much higher than in the former one, but this involves the concomitant risk of, for example, concentrated chlorine solution attacking the unprotected concrete of the pipe's inside wall. A protection coating can be provided for a specific distance downstream of the dosing point, but whereas there is plenty of published material on jet trajectories close to the nozzle and downstream diffusion rates in the far field, the author knows of none in the public domain that gives any indication of how far downstream a protective coating needs to be provided.

Because most of the applications in this sense are of a civil engineering nature, where full-scale testing is expensive, this article therefore reports the results of a computational fluid dynamics (CFD) approach to predicting contaminant concentration levels on a pipe wall at high Reynolds numbers. This gives the bonus of providing also some high Reynolds number predictions for jet trajectories, most published results being for somewhat lower values. Comparison is then made with these experimental results for jet trajectories and for contaminant concentrations at locations well downstream to validate the CFD predictions.

Where possible, a nondimensional approach is adopted so that results can be used more widely as a design guide. Three nozzle diameters and a considerable range of jet to pipe flow velocity ratios have been used to obtain as comprehensive a picture as possible and pipe Reynolds numbers of around a million apply.

Address reprint requests to Professor Neve at the Thermo-Fluids Engineering Research Centre, Department of Mechanical Engineering and Aeronautics, City University, London, EC1V 0HB, UK.

Received 2 March 1993; accepted 17 May 1993

Jet and main flow interaction

The earliest work relating to this subject was reported by Goldstein et al. (1968) who investigated the interaction between a circular jet and a free stream. The application in view was the film cooling of gas turbine blades by the dumping of cooler air from small holes in the blade surfaces. Effectiveness is then measured in terms of the local surface heat transfer rate so that some advantage is gained in ensuring maximum interaction between jet and surface. Further work was necessary to investigate the jet to free stream density ratios (Goldstein et al. 1974; Pedersen et al. 1977) because the injected air is inevitably cooler and typically twice as dense.

Major work by Foster and Lampard (1975), Foster (1976) and Foster and Lampard (1980) has dealt with geometrical considerations associated with rows of holes and a density ratio of 2, and recent work by Sinha et al. with a single row of holes and various density ratios (1991b) and with two rows of holes (1991a) gives the most up-to-date picture. Foster and Lampard (1980) showed a relationship between effectiveness and jet injection angle (relative to the plate), blowing rates and upstream boundary layer thickness and velocity profiles. Shallow injection angles were best for low blowing rates but larger angles (including 90°) for high values. They found that reduction in effectiveness with increased blowing rates was usually associated with increased lateral mixing and not necessarily because of deeper jet penetration of the free steam.

Sinha et al. (1991b) used a single injection angle of 35° and density ratios from 1.2 to 2. They found that jets could normally detach themselves from the surface when their momentum flux per unit area was more than about 70 percent that of the free stream. Further, this momentum ratio seemed to be a variable against which the results for effectiveness could be normalized. At lower ratios, where the jet remained attached to the surface, normalization was best achieved using mass flow ratio rather than momentum.

These last points should be borne in mind in what follows, but it must be emphasized that the research described so far has had as its goal the maintenance of an interaction between a jet and a wall, whereas the current work has the different aim of efficient mixing of jet and free stream without a major contaminant concentration near a wall. In the case of film cooling, the coolant mixing layer rarely rises more than about six nozzle diameters above the surface, whereas the current work involves an interaction with the whole pipe flow.

The issuing of a jet from a wall, radially into a pipe flow, has been extensively researched and there seems general agreement that the subsequent process of aligning itself with the main flow can be split into three distinct regions. In the first, there is little bending of the jet axis and its inviscid core is eaten away by turbulent mixing, much as it would be if issuing into a stationary fluid. This region is only a few nozzle diameters long.

In the second region, the jet axis deflects noticeably, and the centerline speed degrades as the jet mixes with the bulk fluid. Two counterrotating vortices are formed at the jet's edge, much as they would be if a solid cylinder had been placed in the flow, but this particular "cylinder" has a curved axis and the vortices' axes are therefore also curved. The jet's velocity contours, viewed from along its axis, are now reniform in shape, and the two associated vortices are beginning to cause a marked interaction with the bulk flow. From simple momentum considerations, the jet's trajectory clearly depends on the ratio of jet to pipe flow momentum fluxes, but two extremes are worth considering.

(1) At low values of this ratio, the two contrarotating vortices do not form properly (Kamotani and Greber 1972), and mixing rate is therefore presumably controlled more by the ambient pipe flow turbulence levels.
(2) At high MR values, the jet "bounces off" the opposite pipe wall (Guven and Benefield 1983; Kamotani and Greber 1972; Maruyama et al. 1981), and its maximum penetration of the pipe flow is thus limited by the pipe diameter.

Case (1) is possibly similar to Sinha's phenomenon, described previously, of the jet adhering to the wall.

In the third region, jet deflection is largely complete, and its axis is parallel to that of the pipe. Mixing of the contaminant and the pipe fluid is now controlled by the two counterrotating vortices and the ambient fluid turbulence intensity but the distribution of the contaminant approaches uniformity only gradually and asymptotically.

The parameter defining the uniformity of distribution is universally taken to be the standard deviation of the concentration level C over a pipe cross section divided by the space mean value at that section, considering mass flow rate.

$$C_V = \left\{ \frac{\int (C/\bar{C} - 1)^2 V \cdot dA}{\int V \cdot dA} \right\}^{1/2} \quad (1)$$

In Equation 1, the densities of the two flows have been taken to be equal and that applies throughout this article.

The first two regions delineated previously are usually referred to as the near field and the third as the far field; this terminology is also used.

Near field

The near field flow phenomena have been extensively researched, but normally at Reynolds numbers an order of magnitude lower than is applicable in many civil engineering fields. Kamotani and Greber (1972) investigated trajectories using air and a small jet diameter (6.35 mm) in a square-section duct, the jet Reynolds numbers being between 2,800 and 4,200. Their results agree well with those of Margason (1968), although the latter show considerable scatter. In the current notation, the jet trajectory is given by

$$y/D_n = 0.89\,(VR)^{0.94}(z/D_n)^{0.36} \quad (2)$$

VR values from 4 to 8 were used for detailed investigation of trajectories, and their figures show that twin vortices develop strongly in the latter case but hardly at all in the former. For less detailed trajectory studies, VR values up to about 24 were used. Many authors adopt a relationship similar to Equation 2, as might be expected from dimensional analysis considerations, and much of their work has been reviewed in an excellent article by Guven and Benefield (1983). If Equation 2 is recast in more general form,

$$y/D_n = \text{Constant}\,(VR)^m(z/D_n)^n \quad (3)$$

the results can be summarized, in terms of m and n, as in Table 1.

Some authors have referred to momentum ratio as well as velocity ratio in dealing with trajectories. This is logical and in keeping with the data from film cooling, because the process is essentially one of momentum interaction so Equation 3 could equally well be recast in terms of MR, because this parameter

Notation

A	Area
C	Contaminant concentration (percent of initial value in nozzle)
$\bar{C}$	Cross-sectional mean value of C
C_V	Coefficient of variation (Equation 1)
D	Diameter
DR	Ratio of nozzle to pipe diameters
f	Darcy friction factor ($= 8\tau_w/\rho\bar{V}^2$)
I	Intercept value (Equation 5)
k	Turbulence kinetic energy per unit mass
L	Dimensionless distance downstream ($= z/D_p$)
MR	Ratio of jet to pipe flow momenta
R	Pipe radius
Re	Reynolds number ($= \bar{V}D\rho/\mu$)
r	Radius measured from pipe axis
V	Fluid speed in streamwise direction
$\bar{V}$	Cross-sectional mean value of V
VR	Ratio of jet to pipe flow velocities
y	Radial distance from wall
z	Axial distance from jet nozzle center

Greek symbols

μ	Fluid dynamic viscosity
ρ	Fluid density
ε	Turbulence dissipation rate
τ	Shear stress

Subscripts

j	Jet
max	Maximum value
n	Nozzle
p	Pipe
w	Wall

Table 1 Summary of results, in terms of m and n, of Equation 3

Reference	Value of m	Value of n
Kamotani and Greber (1972)	0.94	0.36
Broadwell and Breidenthal (1984) (theor.)	2/3	1/3
Pratte and Baines (1967)	0.72	0.28
Wright (1977)	2/3	1/3

is linked to VR through the diameter ratio DR. The suggestion is made, in some cases that an optimum value of MR exists, in the sense that deflection of the jet as far as the pipe axis will result in most rapid mixing. This is not obviously true because ambient turbulence is lowest on the pipe centerline. Results given by Laufer (1954) show that in the range $5 \times 10^4 < \mathrm{Re} < 5 \times 10^5$, relative turbulence intensity increases from about 3 percent on the axis to about 8 percent near the wall (but outside the area where the presence of a solid wall damps out the turbulence fluctuations). Suggestions for optimum MR are 0.0156 from Ger and Holley (1976) and 0.013 from Fitzgerald and Holley (1981), but their diameter ratios were both very low at about 0.02. For a very high value of DR of 0.285, Chilton and Genereaux (1930) suggest an optimum condition of $VR = 2.7$, which converts into an MR value of 0.592. This difference between optimum performance for small and large nozzles will become more evident later in this article.

Two analytical approaches have been made to this problem. Adler and Baron (1979) use an integral method. Two integral momentum equations are set up, one for each of the directions parallel to, and perpendicular to, the jet centerline. The entrainment rate is taken to be the linear sum of those resulting from straight circular jet and a vortex pair. Their predictions agree well with the experimental results of Kamotani and Greber (1972). Broadwell and Breidenthal (1984) eschew that approach and concentrate more on the vortex pair. Their prediction for the trajectory has already been shown in Table 1 and is supported (numerically) by the general level of experimental figures in that table.

It is important to point out here that all the authors in Table 1 were concerned with either rectangular ducts or "unbounded" flows. There is therefore no (D_n/D_p) term in Equation 3, but this must clearly be an important parameter in considering jet trajectories in pipes. The following candidate equation is therefore put forward:

$$y/D_n = \mathrm{Constant}(VR)^m(z/D_n)^n(DR)^p \quad (4)$$

It was one of the aims of this exercise to find the value of p. The overriding problem, however, was to use a CFD technique to assess the contaminant concentration levels on the walls close to the dosing point (Figure 1).

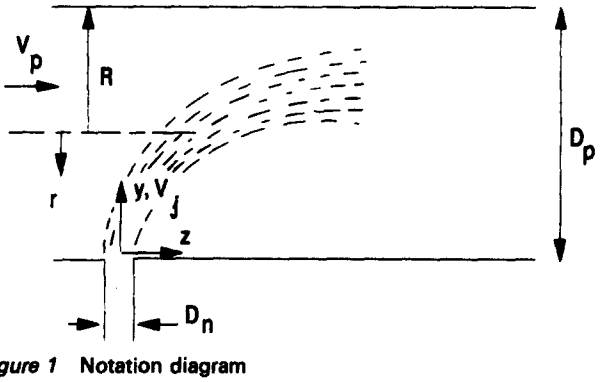

Figure 1 Notation diagram

Far field

The degradation rate of C with downstream travel in the far field has received less attention than trajectories in the near field, but published results will be useful here, especially in the sense that CFD predictions can then be validated by comparison with them. The coefficient of variation C_v attains a value of 0 (i.e., perfect mixing) asymptotically and only at infinity so experimenters rely on the accuracy of their measuring techniques to specify when mixing might be considered effectively complete. Lower limits are quoted by Fitzgerald and Holley (1981) as being 0.05 for fluorescent tracer methods, 0.02 for conductivity, and 0.003 for radioactive tracers. Taking 0.02 as a guide value, it is generally agreed that at least 150 pipe diameters of travel are needed for C_v to decline to that value so the far field mixing process is not particularly rapid.

Using the equations of flow in cylindrical polar coordinates and experimental results for some of the constants involved, Ger and Holley (1976) derived an equation for C_v in terms of the dimensionless distance downstream L $(= z/D_p)$ and the Darcy friction factor f $(= 8\tau_w/\rho\bar{V}^2)$:

$$C_v = I/10^{(L\sqrt{f})/12.1} \quad (5)$$

I is a dimensionless intercept from their derivative graphs and is a function of MR, but their graph of I versus MR has very considerable scatter. However, this will be found useful later, for comparative purposes. Fitzgerald and Holley (1981) extended this work to injection angles other than 90° and to adding a whirl component at injection.

Edwards, Sherman, and Breidenthal (1985) extended the approach of Broadwell and Breidenthal to the far field problem and carried out tests using gases at very small scale. Their results gave the equation

$$C_v = 0.4/MR(z/D_p) \quad (6)$$

and, although their Reynolds numbers were much lower than anyone else's, this relationship will be found to be in very good agreement with some of the CFD results.

Mathematical modeling procedure

The PHOENICS program was used for the mathematical modeling of a water jet issuing radially into a main pipe. This is a finite volume technique, using linearized versions of the flow equations and solving by iteration over a slab of cells perpendicular to the bulk flow direction. After a specified number of iterations, the solution procedure moves to the next slab of cells downstream and so on to give a "sweep" of the whole grid. In this case, 100 such sweeps were used to obtain more than adequate convergence. A cylindrical polar grid was used, making use of the vertical plane of symmetry through the dosing point.

Grid fineness tests were carried out in the direction of most rapid change (radial), and justification will be given in the discussion section for using no more than 20 cells across the radius. The final grid had 20 (radial) × 10 (circumferential) × 26 (axial) cells and the pipe length was variable from 12 to 400 m to give the sensitivity required for various parts of this investigation. Pipe diameter was set at 4 m, water speed at 0.25 m/s (to give $\mathrm{Re} \doteq 10^6$), and jet speed was able to be set at various multiples of the main pipe speed. Nozzle diameters used were 150, 300, and 450 mm.

Turbulence was modeled using the $k - \varepsilon$ method, which has been found particularly effective for high Reynolds number applications. Runs were undertaken on a Sun Sparcstation, the

average time taken for 100 sweeps being about 1,190 s, just under 20 min.

Results analysis

Grid fineness

Initial runs were made with no jet injection, and the grid stretched to 100 diameters long to give a fully developed pipe flow profile for velocity and turbulence parameters. These profiles were then used as inputs for the runs involving jet injection. Grids having 20, 30, and 40 cells in the radial direction were used, and the results are shown in Figure 2. The additional computing time required for the 30- and 40-cell cases would seem not to be justified because the velocity profiles are virtually identical. The 20-cell grid was therefore adopted. The effect of Reynolds number was shown by running at 1 m/s water speed, and Figure 2 shows a slightly fuller profile for that case, as would be expected. A logarithmic plot of this graph would show that the profile is of the $1/n$ power-law type with n, in this case, being about 9; once again, this is what one would expect at very high Re. The predicted pressure drop for the 0.25 m/s cases gave a Darcy friction factor f of 0.0118; this is consistent with a relatively smooth surface at $\mathrm{Re} \simeq 10^6$.

Pipe turbulence

Figure 3 shows the computed k values across the pipe radius for both main flow speeds and all three grids at the lower speed. Once again, there is no obvious point in using more than 20 radial cells.

k is the kinetic energy per unit mass of the turbulent fluctuating components so its square root is directly proportional to the local turbulence intensity. A k value of 0.0003 m^2/s^2 near the wall corresponds to a turbulence intensity of 9 percent, very close to Laufer's value of 8 percent. The trend to Laufer's figure of 3 percent at the pipe axis is also seen. His results were obtained at Reynolds numbers up to about half a million so the PHOENICS program would seem to be predicting the turbulence generation rate quite accurately. The results for a water speed of 1 m/s are shown on a separate axis, and although the predicted intensity is still about 9 percent (the denominator is now 1 m/s, four times greater), it would be noted that the actual k values, a measure of the absolute turbulence levels, are quite different.

The velocity and turbulence distributions from Figures 2 and 3 were used as the input conditions at each of the 20 radial

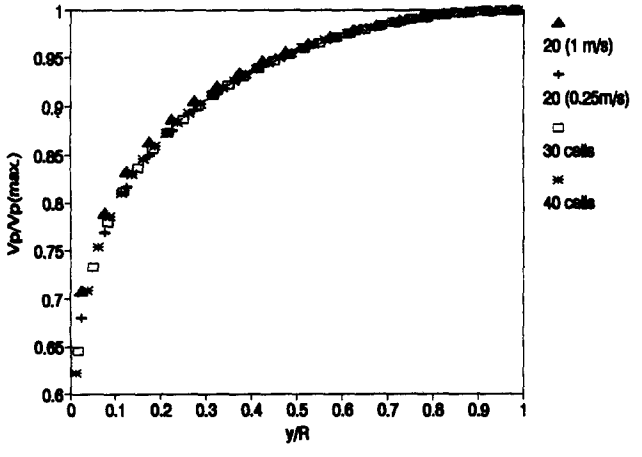

Figure 2 Grid fineness tests—effect on axial velocity profile

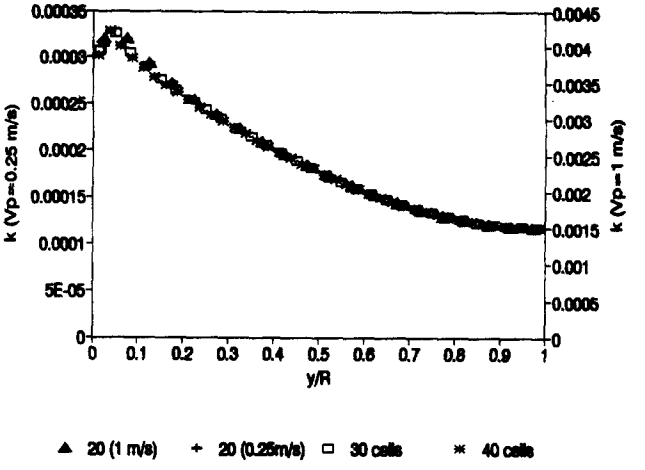

Figure 3 Grid fineness tests—effect on turbulence parameter k

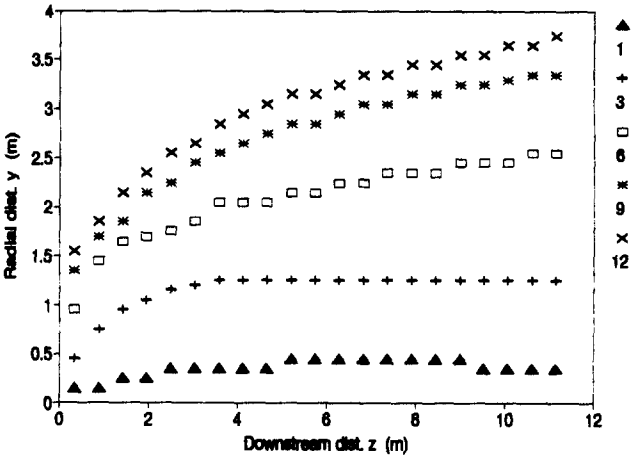

Figure 4 Jet trajectories for 150-mm nozzle (legend shows velocity ratio VR)

grid stations for the main computer runs, the results from which are described subsequently.

Jet trajectories

The predicted trajectories for a 150-mm nozzle diameter and various jet to main flow velocity ratios are shown in Figure 4; in each case, the locus of the highest C value is plotted. The curves range from that for a VR of only one, where the jet penetrates to only about one-eighth of the pipe diameter and then seems to fall again, to the $VR = 12$ case, where the jet is so powerful that it is obviously going to interact with the opposite wall. The former case is broadly in agreement with the results of Sinha et al. (1991b) where the jet would remain attached if the velocity ratio were low enough, about 0.76 in Sinha's case. The trajectories for the other jet to pipe diameter ratios were clearly different, but logarithmic plotting of all cases where the jet did penetrate well into the pipe flow was undertaken to determine the best-fit values for the indices in Equation 4. The result is shown in Figure 5, the agreement being reasonable for a range of jet to pipe momentum ratios of about 9:1. The CFD version of Equation 4 was found to be

$$y/D_n = 0.74\,(VR)^{0.67}(z/D_n)^{0.25}(DR)^{-0.25} \qquad (7)$$

This agrees most closely with the experimental results of Pratte and Baines, given in Table 1, and contains the additional

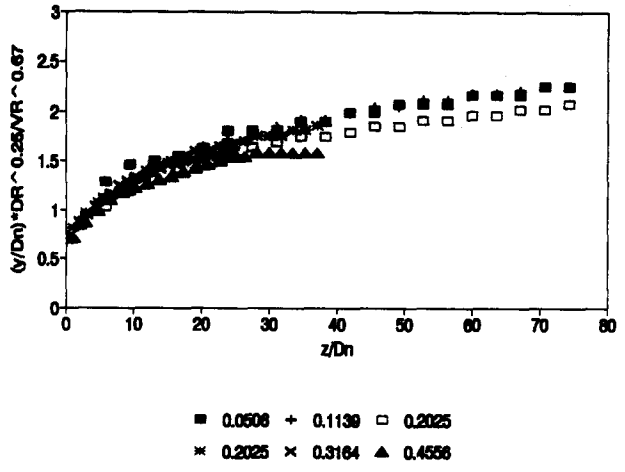

Figure 5 Dimensionless trajectory plots; (legend shows momentum ratio *MR*)

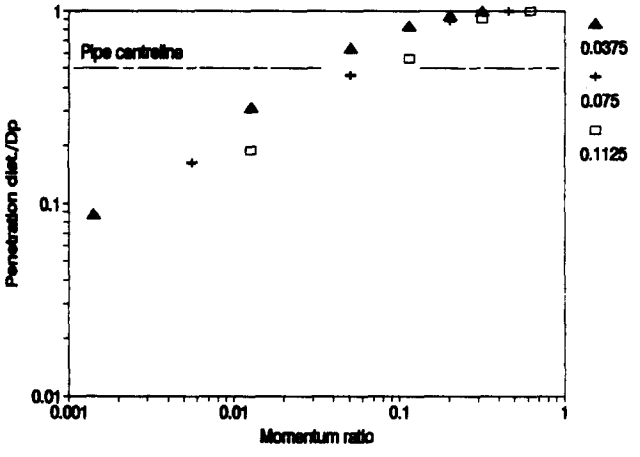

Figure 6 Jet penetration distance at $z = 12$ m (legend shows diameter ratio *DR*)

function of diameter ratio, which did not apply to their rectangular duct case. Because momentum ratio is equal to $(VR)^2(DR)^2$ (for equal fluid densities), Equation 7 can be recast in terms of MR and D_p, which is in some cases more immediately useful.

$$y/D_p = 0.74\,(MR)^{0.333}(z/D_p)^{0.25}(DR)^{-0.17} \qquad (8)$$

It is evident from Figure 5 that the highest momentum ratio case is being affected by the opposite wall, its points prematurely attaining horizontality on the plot. The negative index on the *DR* terms in Equations 7 and 8 implies that a slimmer jet will reach the pipe centerline with a lower momentum or velocity ratio than a wider one, and this is confirmed by Figure 6; the smallest jet reaches the centerline with only about a third of the momentum ratio of the largest one. A quick calculation shows that the largest jet is using about five times the pumping power of the smallest, even though its velocity in the nozzle is only about 58 percent of the other's. Interpolation from Figure 6 enables a comparison to be made with the results of Ger and Holley (1976) and Maruyama et al. (1981). The three data points from the current CFD cases are shown in Figure 7 and appear to act almost as a transition between the two ranges of experimental results of the others.

Contaminant concentration in the near field

The rate of decay of C on the jet centerline should depend on the turbulent mixing characteristics of the jet as if in isolation and on the added effects of interaction with the bulk flow. Raw jet axis values (as percentages of the initial values inside the nozzles) are shown *versus* downstream distance in Figure 8, for three jet diameters and sufficient velocity ratio to propel the jet axis to the central area of bulk flow. There is initially some disagreement, but after about 20 nozzle diameters of travel, the curves seem to settle around the line representing $220/(z/D_n)$, thus indicating that, on a circular jet axis, C degrades in inverse proportion to distance, as centerline velocity is known to do.

Because of an absence of published data, the most important predictions from the present work were to be those of contaminant concentration on the walls, just downstream of the dosing point. In the case of weak jets, the area of interest will clearly be on the wall adjacent to the nozzle, but for strong ones there may also be problems on the opposite wall. Figure 9 shows C (percent) values on the adjacent wall, normalized by multiplication by $VR^{1.3}$. A momentum ratio range of about 30:1 is shown here so scatter can be said to be reasonable, except in the complicated flow region just downstream of the nozzle exit. At very low MR, the ability to normalize with $VR^{1.3}$ is lost, as seen in Figure 10. Although the $MR = 0.00562$

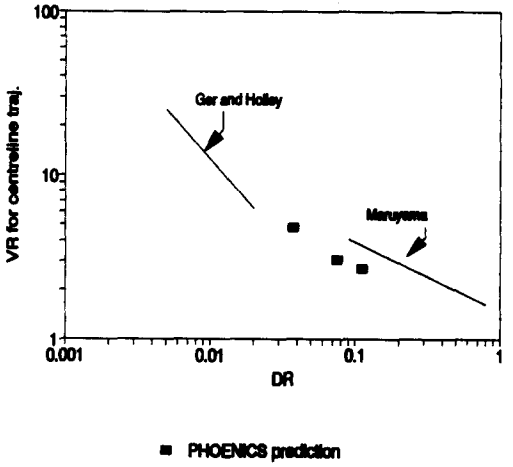

Figure 7 Velocity ratio for jet penetration to pipe centerline; comparison of CFD predictions with published data

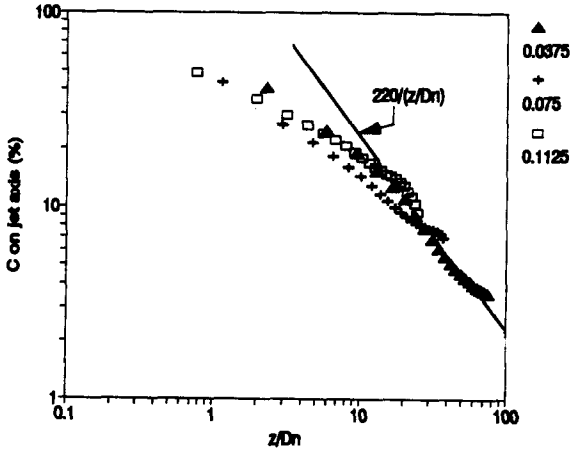

Figure 8 Concentration degradation on jet axis (legend shows diameter ratio *DR*)

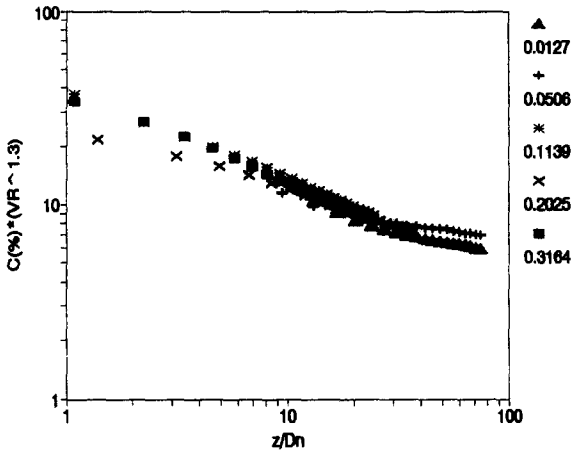

Figure 9 Contaminant concentration on wall adjacent to nozzle (legend shows momentum ratio *MR*)

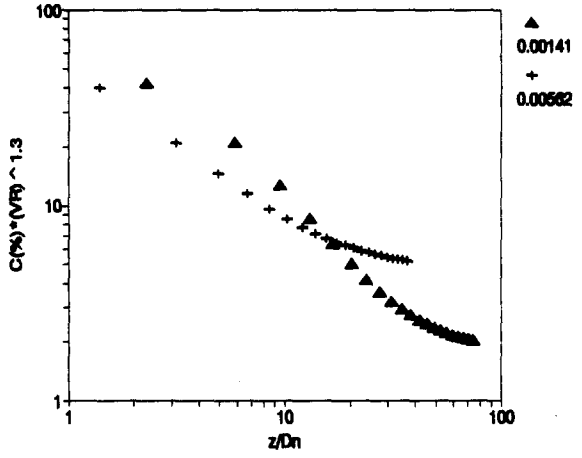

Figure 10 Contaminant concentration on wall adjacent to nozzle (legend shows momentum ratio *MR*)

case bears a strong relationship to the points in Figure 9, the lowest MR of all (0.00141, $VR = 1$, $D_n = 150$ mm) shows wide disagreement. Moreover, C is degrading more rapidly after about 10 nozzle diameters, suggesting vigorous mixing in the wall region.

For high MR values, the concentration on the opposite wall attains some importance. Here it is not so easy to normalize the curves, except by plotting relative to peak values, as seen in Figure 11, but even then the profile similarity is remarkable, except very close to the dosing nozzle. The positions and values of peaks are obtained from Figure 12, where a link with momentum ratio is evident.

$$z/D_p = 1.23/(MR)^{0.734} \tag{9}$$

$$C(\text{percent}) = 151(DR)(MR)^{0.436} \tag{10}$$

The coefficient of variation C_v was introduced earlier as a parameter for indicating how well mixing was progressing. With the aid of a spreadsheet and embedded macros to relieve the drudgery otherwise involved, the computed results can be used to determine C_v at any downstream station, and this is shown in Figure 13. Subsidiary plots show that C_v falls approximately as $(z/D_p)^{0.43}$ so their product can be plotted more or less as a single curve against momentum ratio. Because a lower C_v means more rapid mixing, the trend of Figure 13 is to suggest that greater MR values give some benefits, but this applies, of course, over only the first three pipe diameters.

Far field

To be satisfactorily validated, the modeling program must also predict with reasonable accuracy the degradation of C over

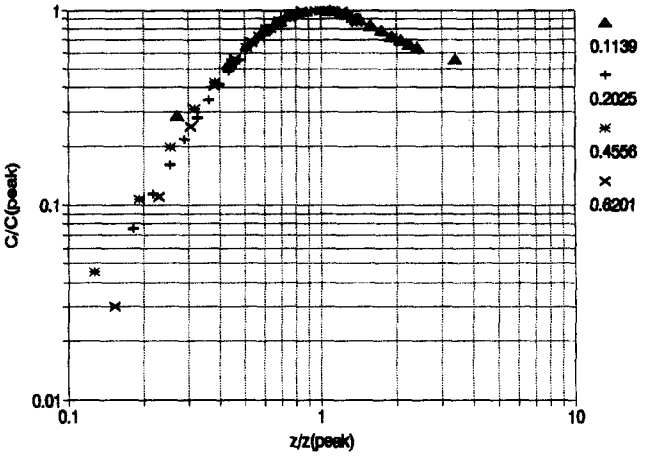

Figure 11 Normalized concentration on wall opposite to nozzle; peak values are given in Figure 12 (legend shows momentum ratio *MR*)

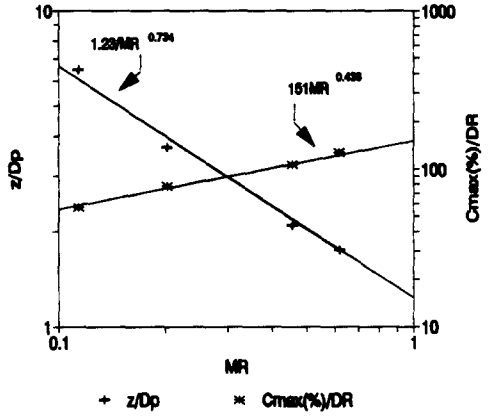

Figure 12 Concentration on wall opposite to nozzle; variation of peak values with momentum ratio *MR*

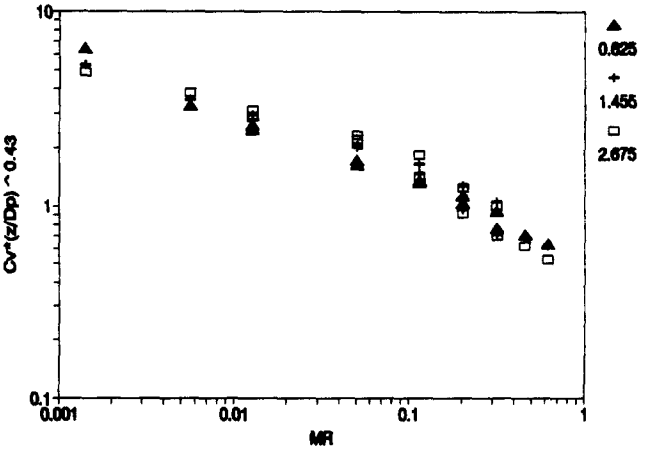

Figure 13 Effect of momentum ratio *MR* on the normalized coefficient of variation C_v in the near field (legend shows downstream distance z/D_p)

considerable distances downstream. Figure 14 shows the result of using progressively coarser grids to determine the value of C_v at up to nearly 100 pipe diameters downstream, and this leaves little doubt that greater momentum ratios lead to faster diffusion of contaminant. Despite earlier signs of promise, the $MR = 0.00141$ case is clearly worst in this figure and the $MR = 0.2025$ case, where the jet was propelled well beyond the pipe axis, reaches the experimentally justified value of 0.02 at $z/D_p \simeq 100$. The apparent incompatibility of the $MR = 0.00141$ points for the far and near field cases may have been caused by the increasing coarseness of the grid in going to greater distances, but this does not seem to have affected the other MR cases.

The results of Edwards, Sherman, and Breidenthal (1985) (see Equation 6) have been superimposed on Figure 14 for $z/D_p > 20$ and agreement between their experimental results and the PHOENICS predictions for $MR > 0.05$ is seen to be very good; this is pleasantly surprising, because their Reynolds numbers were very much lower than those of the current exercise. At lower momentum ratios, the simple Equation 6 is no longer applicable, and either a more involved relationship is required or PHOENICS is no longer predicting the concentration levels with enough accuracy. The approach of Ger and Holley is therefore resorted to, and Equation 5 is fitted to the far field points in Figure 14 to determine the intercept value I, assuming a friction factor of 0.012. Figure 15 shows

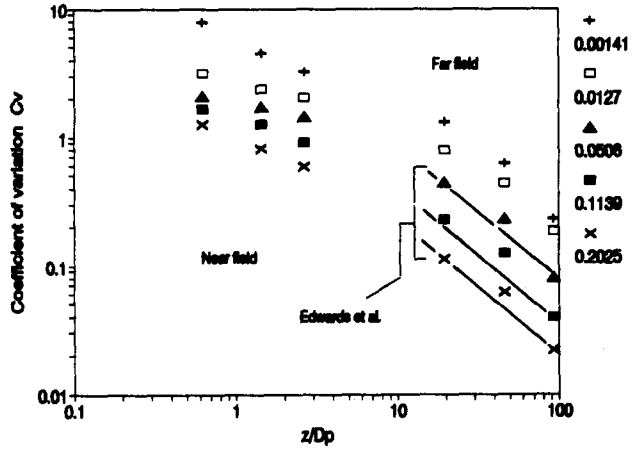

Figure 14 Coefficient of variation C_v in the near and far fields (legend shows momentum ratio MR) (Edwards et al. 1985)

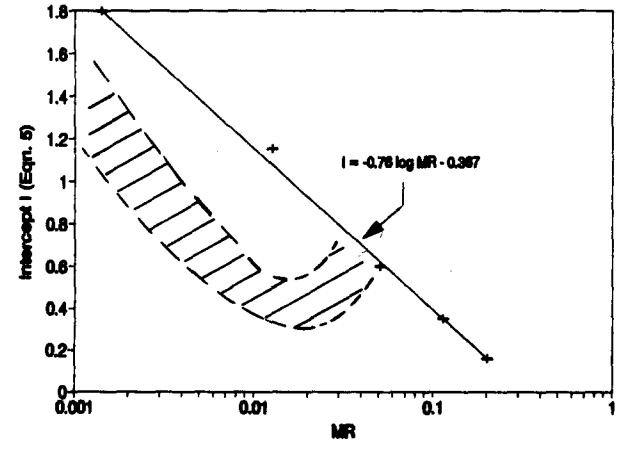

Figure 15 Intercept I (Equation 5) for PHOENICS results; comparison with Ger and Holley (1976) (shaded area)

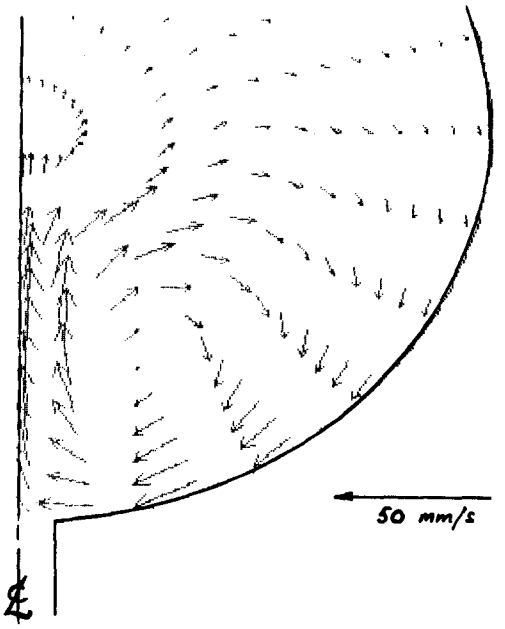

Figure 16 Predicted velocity components normal to the pipe axis at $z/D_n = 16$ ($D_n = 300$ mm)

the result of so doing, and the CFD values of I are clearly higher than those of Ger and Holley, at lower values of MR, even allowing for their considerable scatter. The CFD points fit approximately on the line

$$I = -0.76 \log_{10}(MR) - 0.367 \quad (11)$$

An equation fitting the CFD predictions can therefore be constructed using Equation 11 for I and Ger and Holley's equation for the distance term $(L\sqrt{f})/12.1$.

$$C_v = \{-0.76 \log_{10}(MR) - 0.367\}/10^{(L\sqrt{f})/12.1} \quad (12)$$

Although it does not agree very well with Ger and Holley's results, this equation does nevertheless extend the C_v prediciton facility to low MR values and agrees to within a few percent with Equation 6, which is empirically based, at MR values above about 5 percent.

Graphical output

Although the figures so far presented in this article have been produced from the vast tabulated data output of the PHOENICS program, the PHOTON graphical facility within it can also produce vector and contour plots superimposed on the grid used. Space considerations do not permit more than two examples to be given here.

Figure 16 shows a vector plot of the pipe flow, looking directly upstream at a station 16 nozzle diameters downstream of the dosing point. The grid has been modified to give a clearer graphical output, with 11 radial cells and 14 peripheral ones. The radial cells have been graded, that is, made progressively smaller at increasing radii, to give more information in the outer layers. The velocity components in the plane perpendicular to the flow show quite clearly that the program has satisfactorily modeled the large vortex produced beside the deflected jet; this is, of course, repeated on the other side of the axis of symmetry, by implication. This figure resembles very closely that given for $z/D_n = 20$ for the experimental results of Kamotani and Greber (1972) and once again gives confidence in the modeling technique. Although not shown here, the

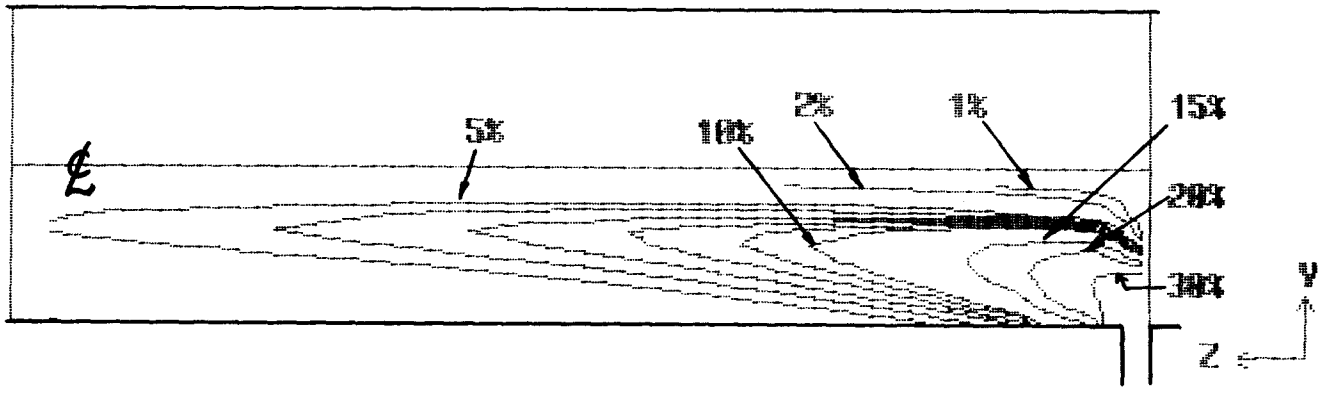

Figure 17 Predicted contaminant concentrations as a percentage of initial value (vertical plane through dosing nozzle)

turbulence intensity distribution also agrees closely with their experiments, producing peaks of more than 20 percent between the large vortex and the pipe centerline.

Finally, Figure 17 shows C contours on the vertical plane through the pipe's centerline, for the same case as Figure 16. The progress of the jet axis is clearly discernible, by implication, from the concentration contours.

Conclusion

The major purpose of this project was to use a CFD procedure to predict contaminant concentration on pipe walls resulting from jet injection, an area where there seems to be little published data, despite its importance. The validity of the CFD predictions was to be assessed against published data for other parameters, where these existed.

The PHOENICS code has clearly predicted jet trajectories with good accuracy, agreeing most closely with the empirical results of Pratte and Baines (1967), but it has also accurately modeled the two contrarotating vortices that are known to accompany the jet interaction with the main flow. This gives confidence that the CFD technique can also predict accurately the contaminant concentration on the walls; Figure 9 can be used by designers to predict wall C values for momentum ratios greater than about 1.3 percent. There is also the implication from the normalization process in Figure 9 that minimum C values on the adjacent walls are obtained with maximum velocity ratio, a result that accords with common sense. As Figure 6 suggests that, for a given momentum ratio, DR should be as low as possible to minimize pumping costs, these various conclusions are seen to be entirely compatible: a designer is best advised to opt for a small diameter, high-speed jet to produce a given momentum ratio.

Conversely, very powerful jets involve the risk of wasting energy in hitting the opposite wall; Figures 11 and 12 should be used in that case. However, this is considered not to be a critical point. Designers using such powerful jets would clearly be expecting high mean contaminant concentrations in the far field, and Figure 11 shows that the peak values on the opposite wall are not going to be vastly greater than these mean values. Pipe protection, if needed for the contaminant concerned, would therefore need to be provided over the whole pipe length.

Figure 14 shows that, irrespective of wall C values, high momentum ratios do seem to lead to most rapid diffusion of contaminant in fluid. The CFD and empirical results are at one here.

References

Adler, D. and Baron, A. 1979. Prediction of a three-dimensional circular turbulent jet in crossflow. *J. AIAA*, **17** (2), 168–174

Broadwell, J. E. and Breidenthal, R. E. 1984. Structure and mixing of a transverse jet in incompressible flow. *J. Fluid Mech.*, **148**, 405–412

Chilton, T. H. and Genereaux, R. P. 1930. The mixing of gases for reaction. *Trans. AI Chem. E.*, **25**, 102

Edwards, A. C., Sherman, W. D. and Breidenthal, R. E. 1985. Turbulent mixing in tubes with transverse injection. *J. AI Chem. E.*, **31** (3), 516–518

Fitzgerald, S. D. and Holley, E. R. 1981. Jet injections for optimum mixing in pipe flow. *J. Hyd. Divn., ASCE*, **107**, 1179–1195

Foster, N. W. 1976. Film cooling of gas turbine blades. Ph.D. thesis, University of Nottingham, UK

Foster, N. W. and Lampard, D. 1975. Effects of density and velocity ratio on discrete hole film cooling. *J. AIAA*, **13** (8), 1112–1114

Foster, N. W. and Lampard, D. 1980. The flow and film cooling effectiveness following injection through a row of holes. *Trans. ASME, J. Eng. Power*, **102**, 584–588

Ger, A. M. and Holley, E. R. 1976. Comparison of single-point injections in pipe flow. *J. Hyd. Divn., ASCE*, **102**, 731–746

Goldstein, R. J., Eckert, E. R. G. and Burggraf, F. 1974. Effect of hole geometry and density on three-dimensional film cooling. *Int. J. Heat Mass Transfer*, **17**, 595–607

Goldstein, R. J., Eckert, E. R. G. and Ramsey, J. W. 1968. Film cooling with injection through holes: adiabatic wall temperatures downstream of a circular hole. *Trans. ASME,, J. Eng. Power*, **90**, 384–395

Guven, O. and Benefield, L. 1983. The design of in-line jet injection blenders. *J. AWWA*, **5** (7), 357–363

Kamotani, Y. and Greber, I. 1972. Experiments on a turbulent jet in a cross flow. *J. AIAA*, **10** (11), 1425–1429

Laufer, J. 1954. The structure of turbulence in fully developed pipe flow. *NACA Tech. Rep.* (No. 1174)

Margason, R. J. 1968. The path of a jet directed at large angles to a subsonic free stream. *NASA Tech. Note* (No. D-4919)

Maruyama, T., Susuki, S. and Mizushina, T. 1981. Pipeline mixing between two fluid streams meeting at a T-junction. *Int. Chem. Eng., AIChE*, **21**, 205

Pedersen, D. R., Eckert, E. R. G. and Goldstein, R. J. 1977. Film cooling with large density differences between the mainstream and the secondary fluid measured by the heat-mass transfer analogy. *Trans. ASME, J. Heat Transfer*, **99**, 620–627

Pratte, B. D. and Baines, W. D. 1967. Profiles of the round turbulent jet in a cross flow. *J. Hyd. Divn., ASCE*, **92**, 53

Sinha, A. K., Bogard, D. G. and Crawford, M. E. 1991a. Gas turbine film cooling: flowfield due to a second row of blades. *Trans. ASME, J. Turbomachinery*, **113**, 450–456

Sinha, A. K., Bogard, D. G. and Crawford, M. E. 1991b. Film cooling effectiveness downstream of a single row of holes with variable density ratio. *Trans. ASME, J Turbomachinery*, **113**, 442–449.

Wright, S. J. 1977. Mean behaviour of buoyant jets in a crossflow. *J. Hyd. Divn., ASCE*, **103**, 499–513